

Modification of turbulent transport with continuous variation of flow shear in the Large Plasma Device

D.A. Schaffner,¹ T.A Carter,¹ G.D. Rossi,² D.S. Guice,¹ J.E. Maggs,¹ S. Vincena,¹ and B. Friedman¹

¹⁾*Department of Physics and Astronomy, University of California, Los Angeles*

²⁾*Department of Physics, University of Texas, Austin*

(Dated: 15 August 2012)

Continuous control over azimuthal flow and shear in the edge of the Large Plasma Device (LAPD) has been achieved using a biasable limiter which has allowed a careful study of the effect of flow shear on pressure-gradient-driven turbulence and transport in LAPD. LAPD rotates spontaneously in the ion diamagnetic direction (IDD); positive limiter bias first reduces, then minimizes (producing a near-zero shear state), and finally reverses the flow into the electron diamagnetic direction (EDD). Degradation of particle confinement is observed in the minimum shearing state and reduction in turbulent particle flux is observed with increasing shearing in both flow directions. Near-complete suppression of turbulent particle flux is observed for shearing rates comparable to the turbulent autocorrelation rate measured in the minimum shear state. Turbulent flux suppression is dominated by amplitude reduction in low-frequency (< 10kHz) density fluctuations. An increase in fluctuations for the highest shearing states is observed with the emergence of a coherent mode which does not lead to net particle transport. The variations of density fluctuations are fit well with power-laws and compare favorably to simple models of shear suppression of transport.

While flow shear does provide a source of free energy for instability and turbulence, it can lead to stabilization of pressure-gradient-driven instabilities and a reduction of turbulent transport in magnetized plasmas^{1,2}. The transport barrier in the high-confinement mode, or H-mode, of tokamak operation³ is attributed to the spontaneous development of an edge flow layer in which strong shearing suppresses transport^{1,2}. The direct connection between the H-mode edge flow layer and improved confinement was first established in experiments on the Continuous Current Tokamak (CCT) in which transport barriers were generated by directly driving edge flow using torque due to radial currents driven by biased electrodes⁴. Biasing has been used to produce improved confinement in a number of subsequent experiments including toroidal devices^{5–7} and linear magnetized plasmas^{8–10}.

While ample evidence for transport reduction in the presence of sheared flow exists^{11,12} and significant effort and progress has been made in developing a theoretical understanding of the interaction between sheared flow and turbulence, there are still a number of open questions that can be answered by experiment. In particular, the exact mechanism behind turbulence modification and transport suppression by shear is still subject to debate: theories present a number of mechanisms including radial decorrelation¹³, nonlinear reduction of turbulent amplitude¹⁴, and modification of turbulent cross-phase¹⁵. Evidence for all of these mechanisms exists in experimental data¹², but a comprehensive experimental dataset establishing in detail the parameter regimes where each mechanism is important has not been acquired. In part, this is due to the fact that most datasets on flow-turbulence interaction come from studies of spontaneously generated flow or in cases where precise external control over flow and flow shear is not possible. A number of basic plasma experiments have utilized biasing techniques to drive flow and flow shear to study flow driven instabilities (e.g.^{16,17}); however, experiments have not been done in which precise external control over flow shear has been achieved in higher-density plasmas with drift-wave turbulence to systematically study the changes in turbulence characteristics and transport.

In this letter, we report on the first experiments in which external control of flow is used to document the response of turbulence and transport to a continuous variation of flow shear, including a zero shear state and a reversal of the flow direction. Shearing rates ($\gamma_s = \partial V_\theta / \partial r$, where $V_\theta = E_r / B$) from zero to up to five times the turbulent autocorrelation rate measured at zero flow shear (τ_{ac}^{-1}) are achieved. Turbulent particle flux is reduced with increasing shearing rate, regardless of the direction of the flow or sign of the flow shear,

with significant reduction occurring for $\gamma_s \sim \tau_{ac}^{-1}$. The observed reduction in particle flux is dominated by a decrease in low-frequency ($f < 10\text{kHz}$) density fluctuation amplitude. For low frequency fluctuations, the crossphase between density and azimuthal electric field fluctuations remain near zero for all shearing rates. With higher shear ($\gamma_s > \tau_{ac}^{-1}$) we observe the emergence of a coherent mode localized spatially in the region of strong flow. Fluctuations from this mode appear to increase density fluctuations above 10kHz, but do not appear to contribute to particle flux.

I. EXPERIMENTAL SETUP

The Large Plasma Device¹⁸ (LAPD) is a 17m long, $\sim 60\text{cm}$ diameter cylindrical plasma produced by a barium-oxide coated nickel cathode. In the experiments reported here, a plasma of density $\sim 2 \times 10^{12} \text{ cm}^{-3}$ and peak temperature of 8eV is produced in a uniform solenoidal magnetic field of 1000G. Measurements of electron density, electron temperature, and potential (both plasma potential and floating potential) are made using Langmuir probes. Measurements of ion saturation current ($I_{\text{sat}} \propto n_e \sqrt{T_e}$) and floating potential (V_f) are taken with a 9-tip Langmuir probe (flush-mount tantalum tips) while temperature and plasma potential are determined using a swept Langmuir probe. I_{sat} fluctuations are taken as a proxy for density fluctuations for the measurements reported in this work. Density profiles are determined by scaling averaged I_{sat} profiles to line-averaged interferometer measurements of density. Turbulent particle flux $\Gamma \propto \langle \tilde{n}_e \tilde{E}_\theta \rangle$ is determined through correlating density fluctuations from one tip of this probe with azimuthal electric field fluctuations (E_θ) derived from floating potential fluctuations on two azimuthally separated tips. Azimuthal $E \times B$ flow is computed using the swept-probe-derived plasma potential. Flows derived using this technique compare very well to measurements using Mach probes⁹ and flows derived from time-delay estimation (TDE) of the velocity of turbulent structures¹⁹.

Biassing experiments have been previously conducted on LAPD in which edge profile steepening and a reduction in turbulent flux was observed^{9,10}. In these experiments, edge flow was driven by biassing the vacuum chamber wall with respect to the plasma source cathode. Transport reduction occurred only for biases above a threshold value. Below the threshold, azimuthal flow was localized near the biased wall and no flow or flow shear was driven in the region where drift wave turbulence exists. Above the threshold, the flow was

able to penetrate radially inward; hence, strong flow and flow shear, with shearing rates far above the low-flow turbulent autocorrelation rate, was driven in the region of strong density gradient. Recent experiments were successful in achieving more continuous control of potential and cross-field flow in the shadow of a small biased obstacle inserted into the LAPD core plasma²⁰. Both confinement improvement and degradation (formation of strong density depletions) were observed with the density profile created by the obstacle in this case.

Motivated by the success of biasing obstacles to control flow, a large annular aluminum limiter was installed in LAPD. The limiter provides a parallel boundary condition for the edge plasma and is biased relative to the cathode of the plasma source to control plasma potential and cross-field flow. The limiter is an iris-like design with four radially movable plates located 2.5m from the cathode as shown schematically in Fig. 2(a). The limiters create a 52cm diameter aperture; downstream of the limiter, plasma on field lines with radial location $r > 26\text{cm}$ has the limiter as a conducting end parallel boundary condition and plasma on field lines for $r < 26\text{cm}$ has the anode/cathode of the source region as a parallel boundary condition. An electrically floating conducting end mesh terminates the plasma on the far end of the device. A capacitor bank and transistor switch supply a voltage pulse to the limiter. The bias pulse lasts 5ms during the flat-top of the $\sim 15\text{ms}$ plasma discharge. The limiter is biased from $\sim 10\text{V}$ below to 50V above the anode potential. Typically, plasma potential in the core LAPD plasma (plasma on field lines that connect to the source region) is very close to the anode voltage and the cathode sits near ground (vacuum chamber wall). The anode potential is above the cathode potential by the discharge voltage, which was $\sim 40\text{V}$ during these experiments.

The effect of biasing the limiters appears to manifest as a change in the plasma potential in the region radially beyond the limiter edge. Fig. ?? shows radial profiles of plasma potential with respect to cathode potential as a function of increasing bias voltage. The anode voltage is indicated as well. The change in potential between the core region (set by the anode) and the limiter region (set by the biasing) results in an electric field in the region of the limiter edge.

Spontaneous azimuthal rotation of the LAPD plasma is observed when the limiters are unbiased (here the limiters are observed to float to a potential $\sim 10\text{V}$ below the anode). In this state, an edge flow (peaked just outside the limiter edge) is observed in the ion

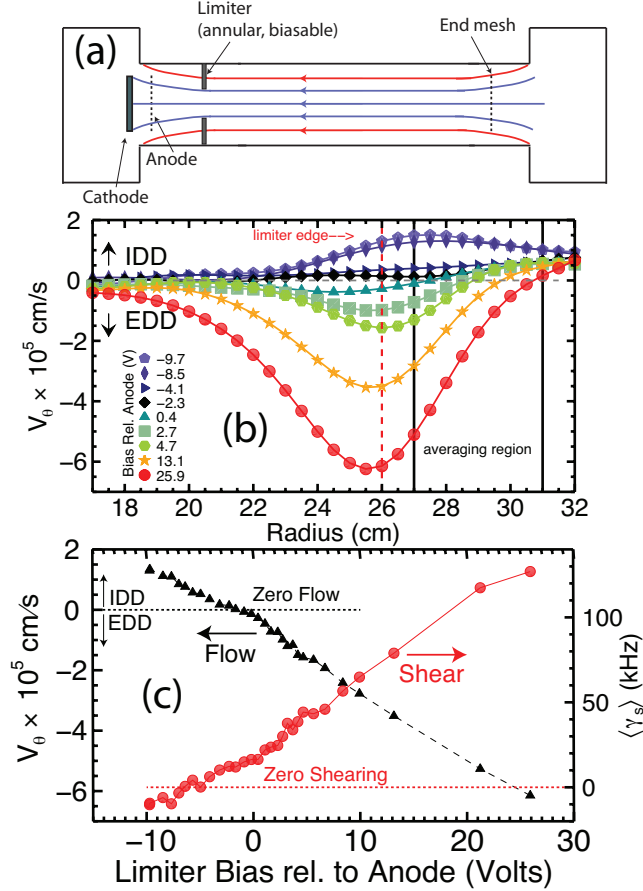


FIG. 1. (a) Diagram of the LAPD device showing annular limiter. (b) Velocity profiles using plasma potential from swept measurements. (c) Flow at the limiter edge (black, triangles) and mean shearing rate, averaged over $27 < r < 31$ cm (red, circles).

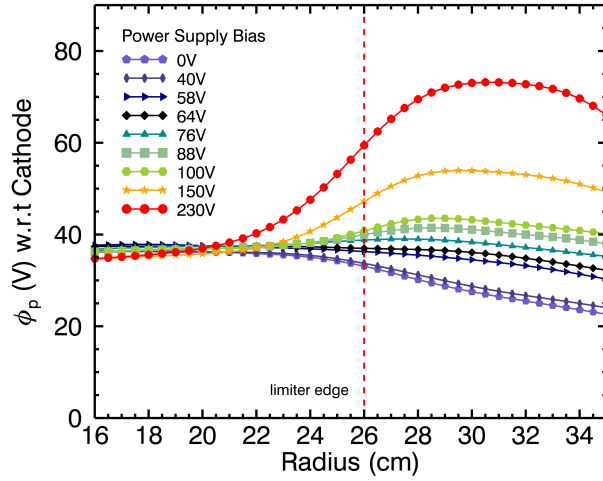


FIG. 2.

diamagnetic drift direction (IDD), as shown in Figure 2(a). Biasing the limiter positively with respect to the cathode tends to drive flow in the electron diamagnetic drift direction (EDD). As the limiter bias is increased, the flow in the IDD is first reduced, then brought to separate near-zero flow and zero flow-shear states, and ultimately reversed with strong EDD flow.

Measurements of profiles of density and particle flux were made for each bias flow state. Values are averaged over a range from $r = 27\text{cm}$ to $r = 31\text{cm}$, a region where average flow and flow shear scale nearly linearly with limiter bias, as shown in Figure 2(b). All other spatially-averaged quantities shown in this paper are averaged over the same region in space.

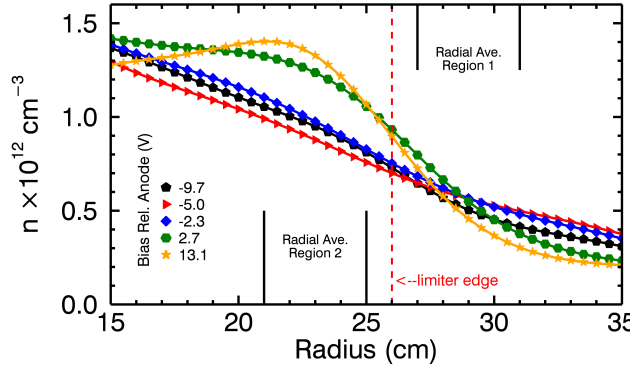


FIG. 3. Denisty profiles.

Fig. 3 shows the density profiles for a range of limiter biases. It is obvious that as the bias reaches its highest values, the density gradient is significantly steepened. Less obvious, but definitely important is that the profile begins in a slightly steeped state (black) but then begins to shallow out when the limiter bias approaches the anode bias (red) before showing significant steepening in the high bias region. This change can be quantified by calculating the average densstiy gradient length scale the radial region indicated.

Figure 4 shows the variation in the spatially-averaged density gradient length scale, $L_n = |\nabla \ln n|^{-1}$ with increasing limiter bias. As the limiter bias is increased, reducing the IDD flow, an increase in the gradient scale length is observed, indicating a degradation of radial particle confinement. The gradient scale length peaks when the averaged shearing rate is near zero. As the bias is increased further, reversing the flow and again increasing the shearing rate, the gradient gradually steepens and the scale length is lowered, indicating improved radial particle confinement.

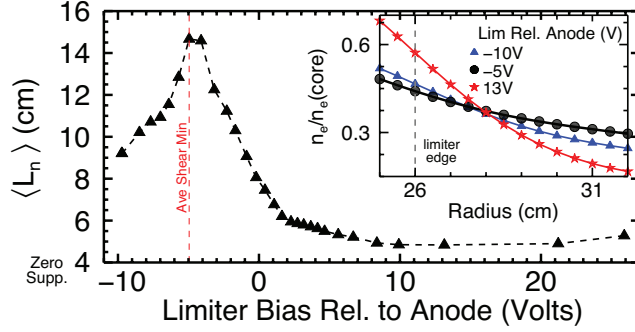


FIG. 4. Density gradient length scale versus limiter bias. Inset shows density profile at three bias values.

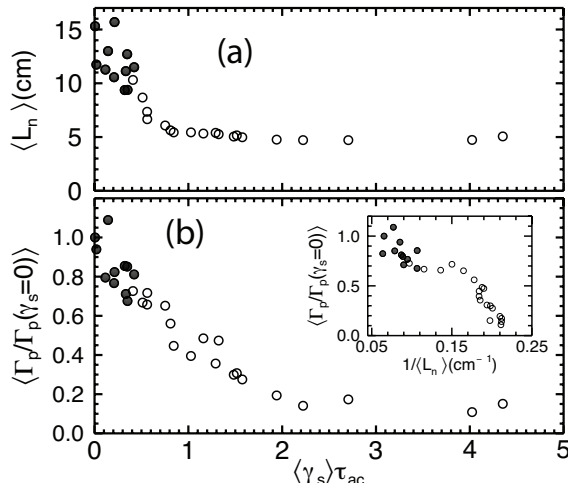


FIG. 5. (a) Gradient scale length versus shearing rate. (b) Particle flux normalized to no-shear flux as a function of normalized shearing rate. Filled symbols represent points with flow in the IDD. Inset: Measured turbulent particle flux versus gradient scale length.

The observed variation of $\langle L_n \rangle$ with bias is best organized when compared to the shearing rate, γ_s , as is shown in Figure 5(a). The shearing rate is normalized to the autocorrelation rate of density fluctuations measured in the zero-shear state. An autocorrelation rate of $\tau_{ac}^{-1} \approx 28\text{kHz}$ ($\tau_{ac} \approx 36\mu\text{s}$) is calculated by taking the half-width at half-maximum of a Hilbert transform of the I_{sat} autocorrelation function. Confinement improvement (decreased $\langle L_n \rangle$) occurs continuously and gradually with increasing γ_s and reaches saturation for $\gamma_s \approx \tau_{ac}^{-1}$ (a normalized γ_s of 1). The profile steepening appears to be largely independent of the direction of the flow (or radial electric field): IDD (filled points) and EDD (open points) flow cases follow the same trend when plotted against normalized shearing rate.

Conversely, the scale length changes do not line up along a single curve if compared

to flow rather than flow shear. Fig ?? shows the same quantities of scale length versus the flow measured at the limiter edge for each bias. Points around the flow minimum are not symmetric; this is physically due to the fact that the minimum shearing rate does not coincide with the minimum flow point. Fortunately this difference allows us to observe the fact that it is flow shear, not necessarily flow, that establishes a maximal density gradient, or minimal confinement.

Measured changes in turbulence and turbulent particle flux are consistent with the observed changes in the density profile. The turbulent particle flux can be written²¹:

$$\Gamma = \frac{2}{B} \int_0^\infty |n(f)| |E_\theta(f)| \gamma_{(n,E_\theta)}(f) \cos[\phi_{(n,E_\theta)}(f)] df \quad (1)$$

where $n(f)$ and $E_\theta(f)$ are the Fourier transforms of the density and azimuthal electric field fluctuations; $\gamma_{(n,E_\theta)}$ is the coherency between density and electric field; and $\phi_{(n,E_\theta)}$ is the cross-phase angle between density and electric field.

Fig 6 shows profiles of these particle flux for varying bias states. The natural state represented by the black curve shows that measured flux peaks in the region of density gradient. As bias is increased, shearing increases and both peak and overall flux increases reaching a maximum at bias 7. Beyond this bias, the flux is generally decreased across the entire radius except for a very narrow region just inside the limiter edge.

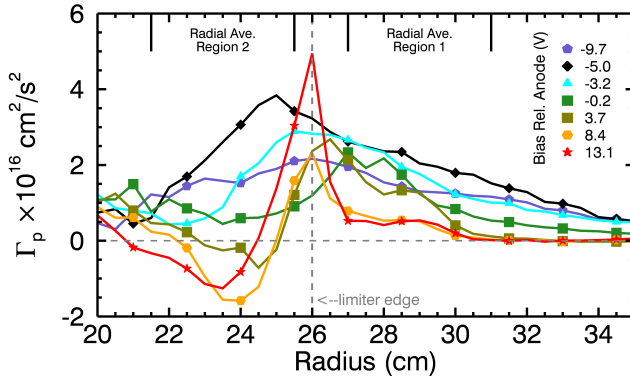


FIG. 6.

In Figure 5(b) shows the spatially-averaged turbulent particle flux as a function of normalized shearing rate. The turbulent flux decreases continuously with increasing shearing rate; however the observed decrease is slightly slower than that observed for L_n . The inset in Figure 5(b) shows that the variation in turbulent flux is correlated with the changes in L_n

(but scales in a way that is inconsistent with Fick's law using a fixed diffusion coefficient). The trend in reduced particle flux is the same for either direction of flow (IDD or EDD). The cause for the reduction in turbulent particle flux can be explored by considering individual terms in the integrand of Eqn. 1.

Density fluctuations were reduced significantly with increasing shearing in these experiments. Figure 7(a) shows changes in the spatially-averaged density fluctuation spectrum with shearing rate. The shearing rate is signed in this figure, and negative shearing rates occur for flow in the IDD. Most of the power is located in frequencies $< 10\text{kHz}$ and in this range, power decreases overall with increasing shearing rate. A decrease of about one order of magnitude in fluctuation power is seen between the minimum shear state and the high shear regime where L_n and particle flux are minimized; this is made clearer in Figure 7(b). At higher shearing rates, $\gamma_s \gtrsim \tau_{ac}^{-1}$, a coherent mode emerges. The frequency of the mode increases with shearing rate and the fluctuation amplitude is localized to the peak of the azimuthal flow.

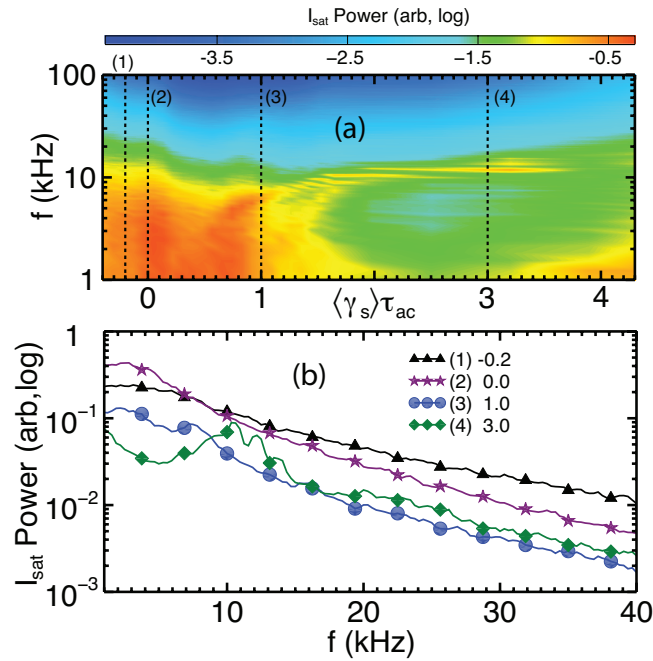


FIG. 7. (a) Contour plot of $\log I_{sat}/\text{density fluctuation power}$ versus shearing rate and frequency. (b) Power spectra for four different values of shearing rate.

Figure 10(a) shows the reduction in total density fluctuation amplitude with shear in two frequency bands: all frequencies below 100kHz in black and all frequencies above 10kHz in

red. With the emergence of the coherent mode, the high frequency fluctuation amplitude does show an increasing trend at higher shearing rates but there is a strong overall decrease in fluctuation amplitude with shearing. A reduction is also seen in E_θ fluctuation amplitude, as shown in Figure 10(b); however this reduction is weaker than observed in density fluctuations. The cross-phase between n and E_θ does not change significantly with shearing. As shown in Figure 10, $\cos[\phi_{(n,E_\theta)}] \sim 1$ for all shearing rates. For higher frequencies ($f > 10\text{kHz}$), the cross-phase does change with shearing, with $\cos[\phi_{(n,E_\theta)}]$ trending toward zero at higher shear. This crossphase change explains why the coherent mode that emerges at higher shearing rate does not contribute to an increase in the particle flux. The coherency between n and E_θ also decreases with shearing rate, as shown in Figure 10. Overall, the decrease in flux is primarily due to a decrease in turbulent amplitude. This observation is distinct from previous work with flows driven by vacuum-chamber-wall biasing on LAPD. In those experiments, turbulent amplitude decreased little while the turbulent cross-phase experienced a significant change, leading to reduced particle flux¹⁰. In the experiments reported here, the magnetic field is higher (1000G versus 400G) and normalized shearing rates are lower (near unity). Cross-phase change is expected in cases with very strong shearing ($\gamma_s \gg \tau_{ac}^{-1}$)²². Future experiments will explore the variation of the turbulent response to higher normalized shearing through changing plasma parameters, in particular magnetic field.

II. TEMPERATURE PROFILES

The electron temperature profiles a measured using triple probe temperature measurements in the core region combined with swept probe temperature measurements in the limiter edge region. Profiles for three different cases were taken as shown in Fig. 9. The black curve shows a typical LAPD temperature profile with a core value of about 8eV with a profile that drops quickly beyond the limiter edge where field lines are no longer connected to the ionization source cathode. About 5cm beyond the cathode edge, the temperature settles to about 2eV consistant with temperatures that would not be expected to produce ionization. For a limiter bias that produces a no-shear, no-flow state, it can be seen that the temperature is modified only slightly peaking to about 9eV just before the limiter edge. This temperature increase is consistant with the expectation for radial biasing current to

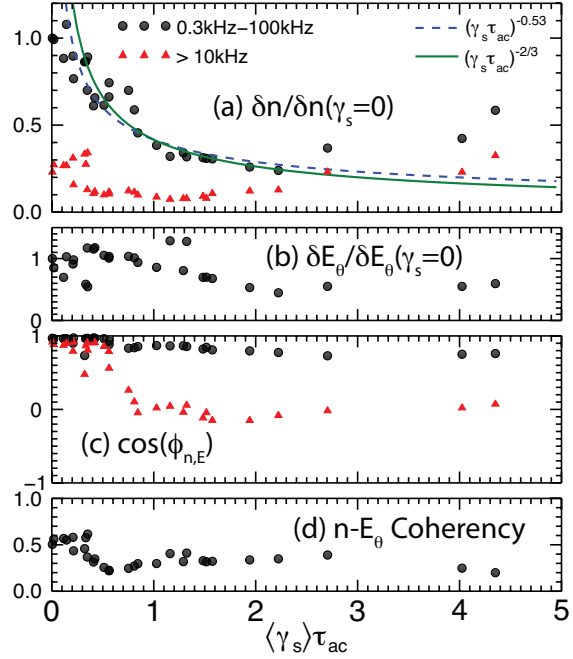


FIG. 8. Components of particle flux versus shearing rate including I_{sat} /density fluctuation power(a), electric field fluctuation power(b), crossphase(c) and coherency(d) with black points for low or all frequency, red for high only.

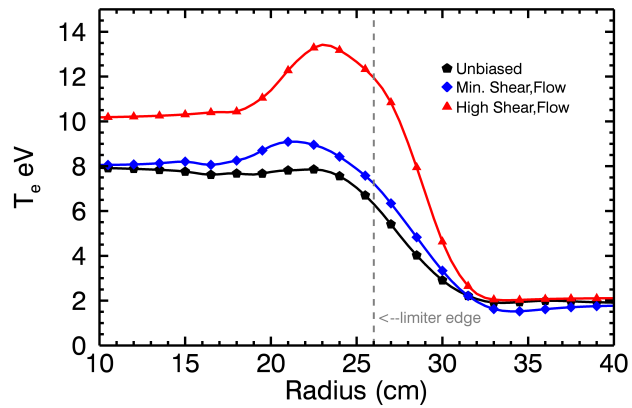


FIG. 9.

be present in this region which could increase the electron temperature locally. The temperature in this no-flow state decreases beyond the limiter edge at a slightly steeper rate, settling to about 2eV at about the same radial distance beyond the limiter edge as in the unbiased case. Finally, a strong limiter bias, producing a strong flow and shear shear state, correspondingly exhibits increased temperature in a similar region just before the limiter edge, maxing out at about 13eV. The increase temperature, again likely due to heating from the injected biasing current, is spread further in this state, increase the core temperature to about 10eV. Beyond the limiter edge, however, just as in the first two cases, the temperature drops substantially and sharply reaching 2eV at the same radial distance as the unbiased and slightly biased cases.

III. FIELD COMPARISON

Plotting flux versus shearing rate for both 1000G and 500G, without normalizing either shearing rate to the autocorrelation rate, shows that flux decreases at nearly the same rate with shearing.

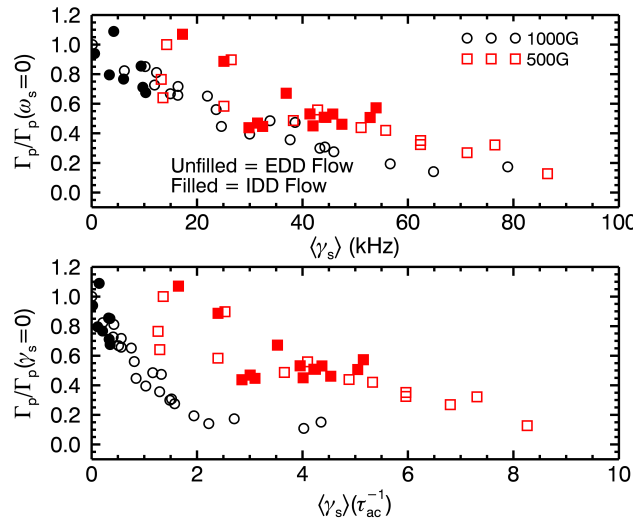


FIG. 10.

IV. MOMENTUM BALANCE

Beginning with the ion azimuthal momentum balance equation,

$$nM \frac{d\vec{V}_i}{dt} = -\vec{\nabla} p_i + \vec{\nabla} \cdot \overleftrightarrow{\pi} + en(\vec{E} + \vec{V}_i \times \vec{B}) + \vec{R}_i \quad (2)$$

where p_i is the ion pressure, $\overleftrightarrow{\pi}$ is the viscosity tensor and \vec{R}_i represents the net force due to collisions with other species. We can assume that the plasma is highly collisional and not fully ionized as is typical for LAPD plasma. Then we can replace the viscosity term with $\vec{\nabla} \cdot \overleftrightarrow{\pi} = \mu_{ii} \nabla_{\perp}^2 \vec{V}_i$ where μ_{ii} is the ion viscosity. The collisionality term, \vec{R}_i , is replaced with $-nM\nu_{in}\vec{V}_i$, where ν_{in} is the ion-neutral collision rate. Finally, we assume that the ion temperature is low enough that a gradient in the temperature can be ignored. On LAPD, an ion temperature of $\sim 1eV$ suggests this can be done. This leaves the balance equation in the form,

$$M \frac{d\vec{V}_i}{dt} \cong en(\vec{E} + \vec{V}_i \times \vec{B}) + \vec{R}_i - M\nu_{in}\vec{V}_i + \mu_{ii} \nabla_{\perp}^2 \vec{V}_i \quad (3)$$

where the density has cancelled out. Using the following cylindrical identities,

$$\begin{aligned} (\vec{A} \cdot \vec{\nabla}) \vec{B} &= \hat{r} \left(A_r \frac{\partial B_r}{\partial r} + A_{\theta} \frac{1}{r} \frac{\partial B_r}{\partial \theta} + A_z \frac{\partial B_r}{\partial z} - \frac{1}{r} A_{\theta} B_{\theta} \right) + \\ &\quad \hat{\theta} \left(A_r \frac{\partial B_{\theta}}{\partial r} + A_{\theta} \frac{1}{r} \frac{\partial B_{\theta}}{\partial \theta} + A_z \frac{\partial B_{\theta}}{\partial z} + \frac{1}{r} A_{\theta} B_r \right) + \\ &\quad \hat{z} \left(A_r \frac{\partial B_z}{\partial r} + A_{\theta} \frac{1}{r} \frac{\partial B_z}{\partial \theta} + A_z \frac{\partial B_z}{\partial z} \right) \end{aligned} \quad (4)$$

and

$$\begin{aligned} \nabla^2 \vec{A} &= \hat{r} \left[\nabla^2 A_r - \frac{1}{r^2} \left(A_r + 2 \frac{\partial A_{\theta}}{\partial \theta} \right) \right] + \\ &\quad \hat{\theta} \left[\nabla^2 A_{\theta} - \frac{1}{r^2} \left(A_{\theta} - 2 \frac{\partial A_r}{\partial \theta} \right) \right] + \\ &\quad \hat{z} [\nabla^2 A_z] \end{aligned} \quad (5)$$

the azimuthal components of the momentum equation are rewritten as,

$$\begin{aligned} M \left(\frac{\partial V_{\theta}}{\partial t} + V_r \frac{\partial V_{\theta}}{\partial r} + \frac{V_{\theta}}{r} \frac{\partial V_{\theta}}{\partial \theta} + V_z \frac{\partial V_{\theta}}{\partial z} + \frac{V_{\theta} V_r}{r} \right) \\ = e(E_{\theta} - V_r B_z) - M\nu_{in}V_{\theta} \\ + M\mu_{ii} \left(\nabla^2 V_{\theta} - \frac{1}{r^2} \left(V_{\theta} - 2 \frac{\partial V_r}{\partial \theta} \right) \right) \end{aligned} \quad (6)$$

Next, a time average is taken of the entire expression. It is assumed these averages have only a radial dependence—that is, there is axial and azimuthal symmetry—and that there is a constant magnetic field while other quantities have the following mean and fluctuating components:

$$\begin{aligned} V_\theta &= \langle V_\theta \rangle + \tilde{V}_\theta \\ V_r &= \langle V_r \rangle + \tilde{V}_r \\ V_z &= \tilde{V}_z \\ E_\theta &= \tilde{E}_\theta \end{aligned} \tag{7}$$

Cancelling terms due to azimuthal and axial symmetry as well as assuming both a steady-state plasma and that fluctuating quantities time-average to zero, the momentum balance equation becomes

$$\begin{aligned} &\left\langle \left(\tilde{V}_r \frac{\partial \tilde{V}_\theta}{\partial r} + \frac{\tilde{V}_\theta}{r} \frac{\partial \tilde{V}_\theta}{\partial \theta} + \tilde{V}_z \frac{\partial \tilde{V}_\theta}{\partial z} + \frac{\tilde{V}_r \tilde{V}_\theta}{r} \right) + \langle V_r \rangle \frac{\partial \langle V_\theta \rangle}{\partial r} + \frac{\langle V_r \rangle \langle V_\theta \rangle}{r} \right\rangle \\ &= -\nu_{in} \langle V_\theta \rangle + \mu_{ii} \left(\frac{\partial^2 \langle V_\theta \rangle}{\partial r^2} + \frac{1}{r} \frac{\partial \langle V_\theta \rangle}{\partial r} - \frac{\langle V_\theta \rangle}{r^2} \right) - \frac{e}{M} \langle V_r \rangle B \end{aligned} \tag{8}$$

If we assume a condition of incompressibility in the plasma, the quantity in the parenthesis on the left hand side of ?? can be written in terms of the gradient of a Reynolds Stress, $R_s = \langle \tilde{V}_r \tilde{V}_\theta \rangle$ so that finally the momentum balance equation becomes

$$\begin{aligned} &\frac{1}{r^2} \frac{\partial}{\partial r} (r^2 \langle \tilde{V}_r \tilde{V}_\theta \rangle) + \langle V_r \rangle \frac{\partial \langle V_\theta \rangle}{\partial r} + \frac{\langle V_r \rangle \langle V_\theta \rangle}{r} \\ &= -\nu_{in} \langle V_\theta \rangle + \mu_{ii} \left(\frac{\partial^2 \langle V_\theta \rangle}{\partial r^2} + \frac{1}{r} \frac{\partial \langle V_\theta \rangle}{\partial r} - \frac{\langle V_\theta \rangle}{r^2} \right) - \frac{e}{M} \langle V_r \rangle B \end{aligned} \tag{9}$$

V. CORRELATION PLANES

Some theories suggest that flow shear is expected to produce radial decorrelation of turbulence, breaking up turbulent eddies into smaller radial scales which in turn results in decreased turbulent fluctuations¹³. We measure the radial correlation length in the plane of the plasma by computing a two-dimensional turbulent correlation functions sing two probes: one probe is held fixed in space (phase reference) and correlating its signals against a second probe, axially separated from the first, which is moved shot-to-shot in a plane perpendicular to the magnetic field. The radial correlation length, Δr_c , is derived from the radial width of the Hilbert transform of the correlation function (half-radial-width and half-maximum at

the location of peak correlation). We can just as easily extract a correlation length in the y-direction, representing the extent in the azimuthal direction. This length can be used for calculating an estimate of the azimuthal wavenumber, k_θ , as well as the azimuthal mode number, M.

Fig. ?? shows the cross-correlation contour plot for three shearing regimes—a)unbiased, IDD flow, b)no-shear, c)high flow/shear—normalized to the maximum correlation within each regime. The reference tip is located at 30cm, just beyond the edge of the limiter and within the spatial averaging region. The most striking change occurs between the no-shear state and a high shear state; the correlation function shifts from a fairly circular shape to radially narrowed and azimuthally elongated structure. In the high bias case, a series of structures can be seen located directly at the limiter edge. This is believed to be a mode-pattern caused by the mode that appears at high bias. Fig. ?? shows the same correlation plane but with the frequencies at which the mode is observed removed leaving the correlation structure unaffected.

Accumulating radial correlation lengths from correlation functions at various shearing states, it can be shown that the radial correlation length decreases with increasing shearing, as shown in Fig. 11.

At higher shearing rate, a coherent mode pattern appears (as shown in the rightmost inset plot) in addition to the primary correlation peak (the coherent mode is pattern shifted inward of the reference probe location which was $r = 30\text{cm}$). The coherent mode does lead to an increasing trend in the radial correlation length at higher shear, but the overall trend is a substantial reduction ($\gtrsim 2$) in the radial correlation length from the no shear state.

VI. WAVENUMBER AND SPECTRAL DENSITY

The azimuthal (or poloidal) wavenumber can be extracted from the probe data using a two-tipped Langmuir probe technique²⁴ (see Appendix?) and combined with frequency information to create spectral density contour plots and with radial distance to calculate distributions of poloidal eigenmodes (M-numbers) present in the plasma. Poloidal eigenmodes—M-numbers—are modified significantly as a function of shearing rate as mode size, mode power and mode direction are all changed over the course of a scan. The countor of Fig. 12a presents a summary of the M-number distribution as a function of bias with cuts show below

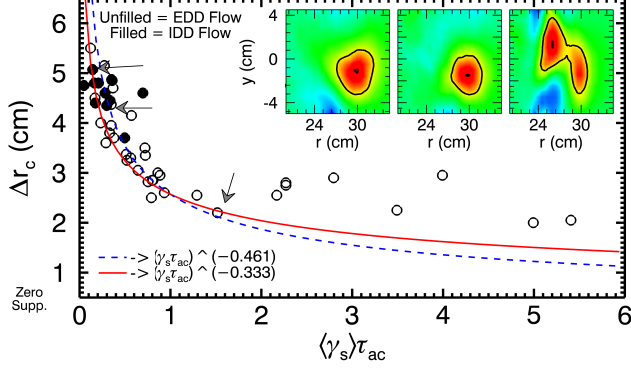


FIG. 11. Δr_c with reference probes at 28,29,30,31 or 32cm with γ_s averaged over measured Δr_c . Inset shows 2D correlation structure for 3 cases: unbiased (spontaneous flow), minimum flow shear and strong EDD flow.

in b) averaged over the same radial range as before, 27 to 31cm. Positive and negative values of M-number are inherited from their corresponding wavenumber, k , which can have a propagation direction. In this arrangement, negative values correspond to modes which propagate in the electron diamagnetic drift direction while positive values are modes propagating in the ion diamagnetic drift direction. Thus, in the unbiased case, it is clear that the dominant modes in this section of the plasma are propagating primarily in the EDD which is consistent with pressure-gradient driven modes. Furthermore, modes of M-numbers 50-60 have the most power associated with them, which is consistent with the structure size found from correlation plane measurements.

As shearing is zeroed, there is a trend toward more power in the EDD modes, again with the peak modes sitting in the range of 50-60. Again this is consistent with the fact that in zero flow and shearing regime, only pressure-gradient modes would be expected to be present. As the flow and shearing is increased just past the no flow region, significant changes begin to be apparent. First, there is an overall reduction in fluctuation power across all modes which reflects the decrease in I_{sat} fluctuation power with shearing rate. Second, the modes that remain begin to be reduced in mode number and more power appears in positive M-numbers. This suggests that as the shearing is increased, the structure size of the turbulence is being elongated in the azimuthal direction which is again consistent with observed correlation plane data. Moreover, the appear of power in the IDD modes suggest the presence of instabilities other than pressure-gradient modes which are not confined to propagate in the EDD—namely, this is highly suggested of the appearance of flow or flow shear

driven modes such as rotational interchange modes or Kelvin-Helmholtz modes.

M-number analysis sheds some light on the mode that appears in the strongly sheared regime. Fig. 13 shows a pure spectral density plot of isat mode frequency versus M-number. The power from each position and bias are stacked. While the majority of the power is located in the EDD propagating modes, there does appear to be a branch that juts out in the IDD. Comparing the frequencies of this branch with that of the mode observed in fluctuation data and correlation plane data suggest that this mode propagates in the IDD and thus would not be a pressure-gradient driven mode.

This same analysis can be cast in terms of a wavenumber versus frequency rather than M-number so that a dispersion relation and phase velocity can be determined. Fig. ?? and Fig. 15 show the summed spectral density plots for low biases (Biases 0-13) and high biases (Biases 14-29). Clearly separate dispersion relations can be calculated for high and low bias regimes, or in other words, regimes for flow in either azimuthal direction. A fit to the peak power wavenumber for each frequency bin gives and estimate of the phase velocity. For low bias, this phase velocity is approximately $1.8 \times 10^4 \text{ cm/s}$ and in the EDD direction while similar fit for high bias yields $v_{phase} = 2 \times 10^2 \text{ cm/s}$ in the IDD direction.

Again, this wavenumber spectral data is highly suggestive of a flow or flow shear driven mode. We can also look at the ratio of floating potential fluctuations to density fluctuations as a metric for determining mode type. Fig. ?? shows profiles of the ratio $\|\frac{\tilde{V}_f}{T_e}/\|\frac{\tilde{n}}{n}\|$, a measure of the relative power in V_f fluctuations versus density fluctuations. For all biases, the ratio hovers around a ratio of 1.0. This appears to limit the type of instability present generally to either rotational interchange or resistive drift waves; that is, the shearing rates produced in all the flow regimes do not appear to be strong enough to drive Kelvin-Helmholtz modes. At the highest biases and near where the flow peaks (at the limiter edge) the ratio begins to drop to 0.5, suggesting a dominance of density fluctuations over potential fluctuations. This is more consistent with the presence of a coherent drift wave rather than a rotational interchange? .

Other methods of distinguishing between drift waves and rotational interchange waves can be by looking at the predicted frequency of the wave, the radial localization of the wave, and the relative phase shift between v_f and density.

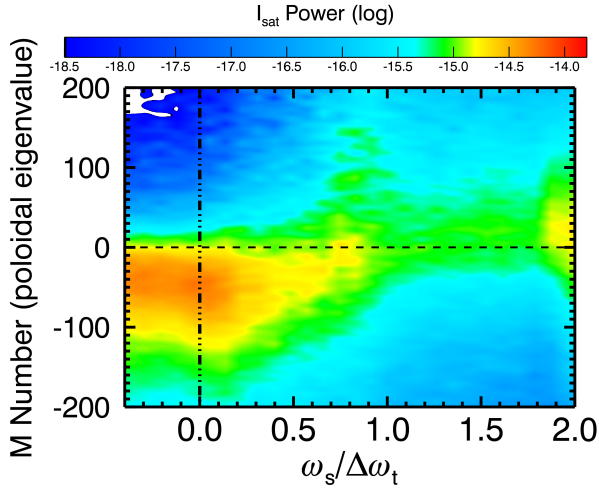


FIG. 12. blah

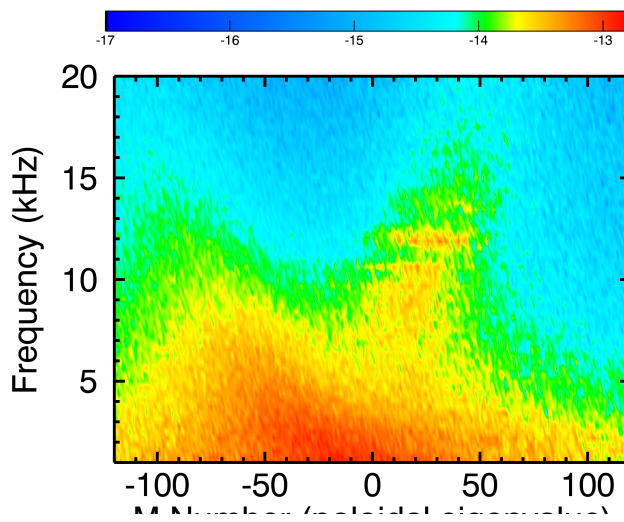


FIG. 13. blah

VII. BIASING CIRCUIT AND SETUP

The biasing circuit consists of a 0.2F, 450V capacitor bank that is pulse discharged through an isolated gate bipolar transistor (IGBT) switch. An 250V, 1.5A Agilent network controlled power supply sets the voltage on the capacitor bank. The discharge circuit, as shown in Fig. 17, supplies a voltage to the limiters through the capacitor bank/IGBT circuit and referenced to the cathode of the plasma discharge circuit. A 0.2Ω wire resistor is placed in series in order to monitor the current of the bias discharge, but the circuit has an overall resistance of about 0.7Ω . Since the discharge current can run into the tens of amperes, the overall voltage applied to the limiters tends to be much less than the power supply can apply

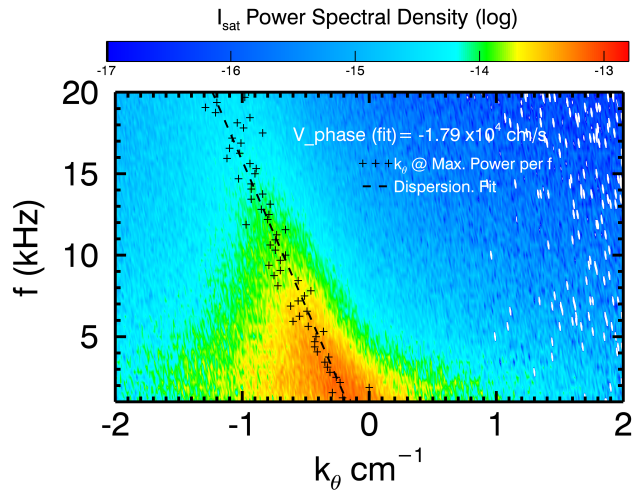


FIG. 14. blah

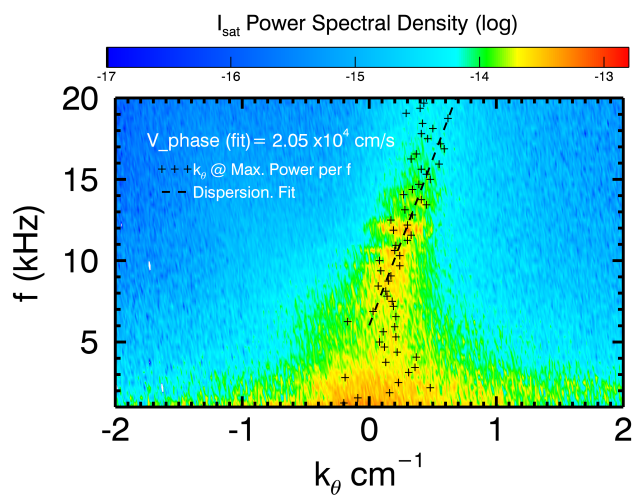


FIG. 15. blah

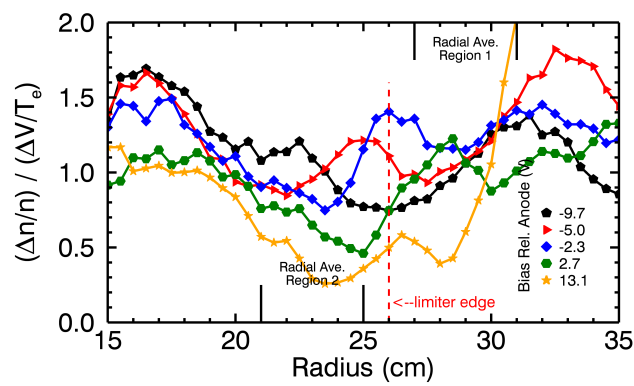


FIG. 16. blah

as indicated by Fig. 17.

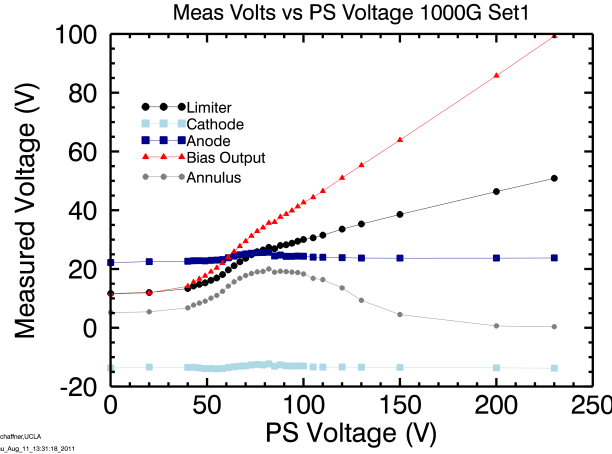


FIG. 17. blah

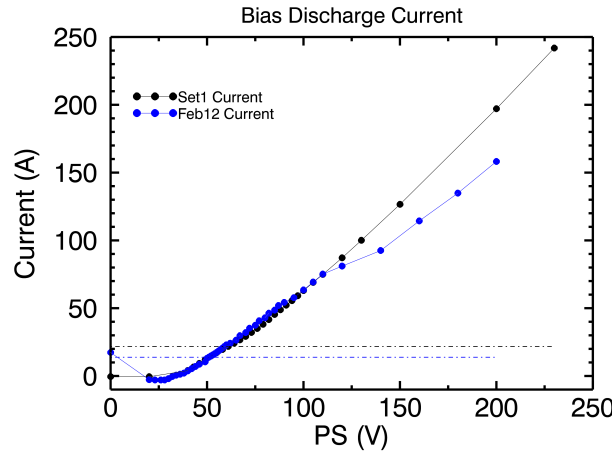


FIG. 18. blah

An I-V curve of the measured current through the biasing circuit as a function of power supply voltage is shown in Fig 18 for two different runs. The curve is Ohmic like for voltages above 30V, with a slope consistent with constant resistance on the order of $1.5\Omega_s$ suggesting that the plasma part of the circuit has a resistance of approximately 0.7Ω . When the power supply voltage is less than the floating potential of the plasma (here about 30V), no current flows.

The anode cathode discharge circuit of LAPD is similar to the biasing discharge circuit in that it is a capacitor bank controlled by an IGBT switch however, the current that is pulsed

through this circuit is on the order of kiloamperes rather than the hundred or so amperes of the biasing circuit. The plasma discharge circuit is also generally isolated from chamber ground so that the discharge voltage difference between the anode and cathode, though fairly constant, can float in reference to chamber ground. For most plasma experiments on LAPD , this is not a big issue as experiments are typically conducted in the core of the plasma and core potential versus boundary potentials do not play a significant role. However, in the biasing experiments, this voltage difference can potentially influence edge flows and so some attempt has been made to fix this issue.

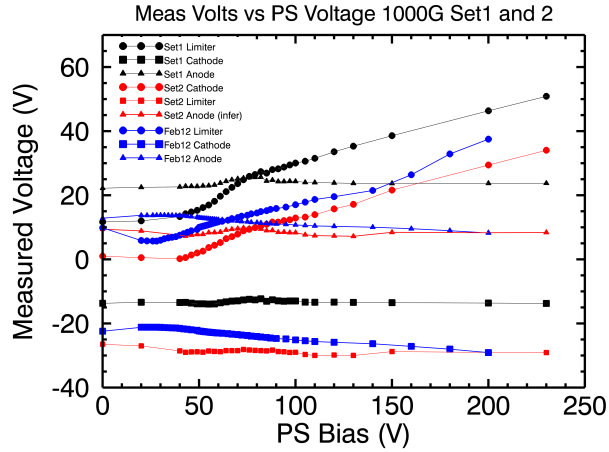


FIG. 19. blah

In these experiments, the cathode is referenced to the plasma ground through a 25W, 2.3Ω resistor with the expectation that the cathode will stay near ground. In practice, however, the cathode typically settles on a potential that is about 10-15V below chamber ground resulting in approximately 5 amperes of current flowing from ground to the cathode. This potential, though, has been observed at many voltages with respect to ground shifting in a range from 5V to 35V below ground over the course weeks and/or months between different run campaigns or even between days within a run campaign as seen in this particular data set shown in Fig. 19 where the first curve was taken approximately two days before the second data set.

This result is somewhat unsurprising as anode-cathode circuit's reference to ground is dependant on the overall current's path to ground. Given a 5kA plasma discharge, approximately half of this current will complete the circuit loop through the anode while the other half will reach ground through the plasma and then through the chamber. A connection

to ground on the order of a few 10s of amps is not likely to make much of a dent in this procedure, but methods for getting the cathode potential controllable are still underway. Fortunately, however, the limiter method of producing flow appears to not be affected by this variability in cathode potential with respect to ground. In these experiments, the flow under most scrutiny is the flow that appears in the region between the core and the limiters rather than between the core and the far chamber edge. Since the limiters are referenced directly to the cathode, the potential differences that matter are those between the cathode, anode and limiters rather than between any of these elements and ground.

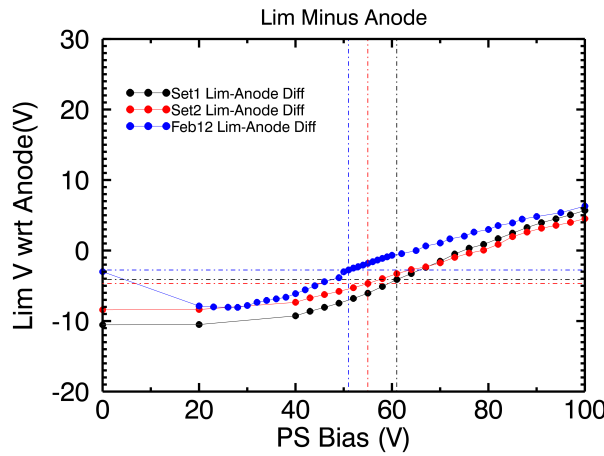


FIG. 20. blah

We can show that while not terrible consistent from run to run, the variations in the cathode potential do not have a significant influence on the flow states under investigation. What about the consistency of the limiter potentials themselves? Figure x shows a comparison of limiter voltage as a function of power supply voltage for three different runs (Sets 1 and 2 are from the same run, two days apart, while Feb12 is from a run eight months after those of Set1 and 2). Though each is offset by a different cathode potential, it is clear that each curve is not exactly the same when plotted as a function of power supply bias. Furthermore, this difference is not alleviated when the cathode/anode potential is accounted for. Fig. ?? shows the difference between anode and limiter voltages as a function of power supply voltage (recall that anode and cathode potential differences are constant with respect to bias).

Even in this case, the curves do not line up. However, an important observation can be made by looking at the density fluctuation data

The data collection for the June 2011 run was done in two main parts. The first part took mach probe flow, triple probe isat, te, and vf, and Reynolds Stress measurements for two fields, 1000G and 500G. The second part took swept plasma potential and te data, 2D flux measurements and B-dot data. In the first set, the voltage of the anode, cathode, limiters, bias output and annulus were monitored while the second set took only cathode and limiter voltage data.

In examining the fluctuation power of one of the 2D Flux probe isat tips from set 2 and comparing it to the power of the isat tip of the triple probe of set 1 it became apparent that there was a slight difference in the features of the contours. A contour plot of log fluctuation isat power as a function of bias number and frequency is show below first for the 2D flux probe data. The power is averaged over the radial range of 27cm to 31cm.

It is clear that a peak in the fluctuation power occurs at about bias 7 which corresponds to the biasing state for the minimum amount of shearing observed. Thus this plot is consistent with the idea that decreased shearing results in more fluctuation power. As one moves away from this bias state in either direction, especially below 10kHz, the overall power decreases showing that power decreases with increased shear. Comparing this plot to a similar one made using triple probe isat data from set 1 shows a slightly different picture.

The appears to be an overall similarity in the changing power going up in Bias Number. There is a peak in fluctuation power at about Bias 9, two biases higher than the flux2D probe, but then the power decreases with increasing bias. Evidence of a coherent mode is also seen in this plot, but it does not seem as distinct as in the Flux 2D data. Also, there appears to be more power in the unbiased state (bias 0) in the range of 5-10kHz than there was in the flux2D data.

Finally, we show the same plot for the density fluctuation data from the February 2012 run.

If we compare the corresponding bias voltages at which the fluctuations peak with the voltage difference between the anode and limiters, as indicated by the dashed crosshairs, there finally appears a consistent metric across runs. That is, the peak density fluctuations, and as has been shown, the minimum shearing regime, occurs when the limiter voltages reaches a value approximately 5V below that of the anode. This presumable can be interpreted as the point where the plasma potential influenced by the anode/cathode boundary and the limiter boundary respectively are equal and thus no flow or flow shear is observed

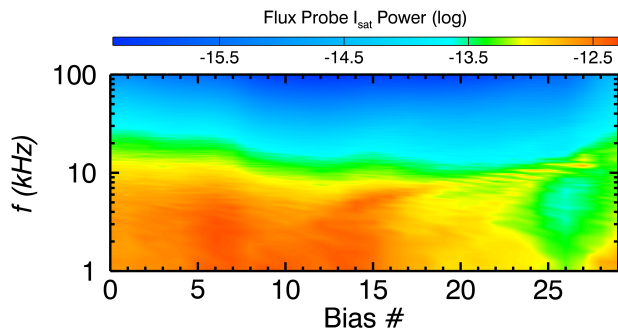


FIG. 21. blah

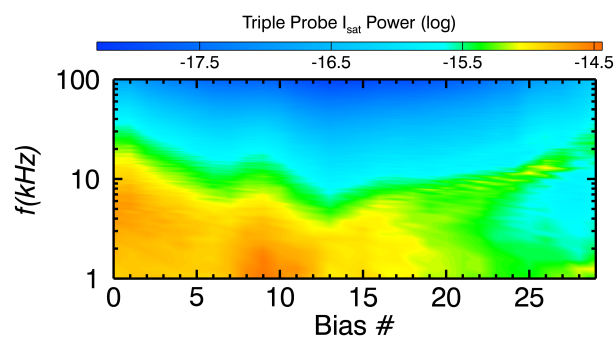


FIG. 22. blah

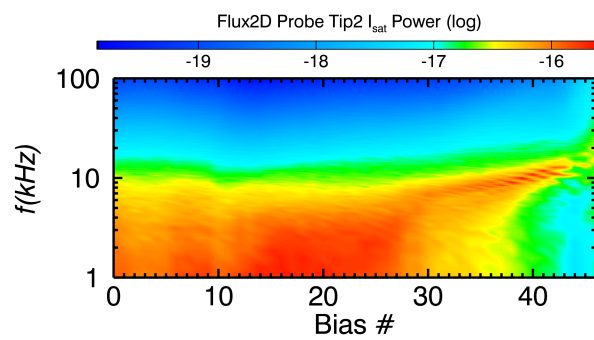


FIG. 23. blah

in the core/limiter edge region. In this way, regardless of how the anode-cathode circuit orients itself with respect to the chamber, or how the limiter potential situates itself with respect to the anode, the minimum shearing point can be located.

VIII. COMPARISON TO THEORY

Lastly, we add a comparison of our data to a simple theory, the Biglari-Diamond-Terry (BDT) model¹³, which predicts a power-law scaling with shearing rate of the turbulent amplitude of the form: $(\gamma_s/\tau_{ac}^{-1})^{-\alpha}$. As seen in Figure 10, a best fit of $\alpha = 0.530$ compares favorably to the BDT prediction of $\alpha = 2/3$ for the reduction in density fluctuation amplitude. It should be noted, however, that the BDT model is fairly simple and the validity of its assumptions is questionable for the experimental conditions reported here. In particular, as the shearing rate is increased in LAPD, the density profile is changing (in BDT a fixed drive is considered). Future work will focus on direct comparisons to more comprehensive models of shear suppression, including comparisons to two-fluid simulations using the BOUT++ 3D turbulence code²³.

This letter presents the first experiments in which the response of pressure-gradient-driven turbulence to a continuous variation of shearing rate, including a near-zero flow shear state and a reversal in the direction of flow, is studied. Increased shearing improves radial particle confinement regardless of the direction of the azimuthal flow or sign of the flow shear. The observed reduction of turbulent particle flux with shear is attributed to a reduction in the amplitude of density fluctuations. These experiments were performed at a fixed set of plasma parameters (fixed magnetic field, neutral pressure, discharge power); future work will explore the variation in turbulent response to shear as these parameters are varied.

REFERENCES

- ¹K. Burrell, Phys. Plasmas **4**, 1499 (1997).
- ²P. Terry, Rev. Mod. Phys. **72**, 109 (2000).
- ³F. Wagner *et al.*, Phys. Rev. Lett. **49**, 1408 (1982).
- ⁴R. Taylor *et al.*, Phys. Rev. Lett. **63**, 2365 (1989).
- ⁵R. Weynants *et al.*, Nucl. Fusion **32**, 837 (1992).

- ⁶J. Boedo *et al.*, Nucl. Fusion **40**, 7 (2000).
- ⁷C. Silva *et al.*, Plas. Phys. Control Fusion **48**, 727 (2006).
- ⁸O. Sakai and Y. Yasaka and R. Itatani, Phys. Rev. Lett. **70**, 4071 (1993).
- ⁹J. Maggs *et al.*, Phys. Plasmas **14**, 052507 (2007).
- ¹⁰T. Carter and J. Maggs, Phys. Plasmas **16**, 012304 (2009).
- ¹¹K. Burrell, Phys. Plasmas **6**, 12 (1999).
- ¹²G. Tynan *et al.*, Plasma Phys. Control Fusion **51**, 113001 (2009).
- ¹³H. Biglari *et al.*, Phys. Fluids B. **2**, 1 (1990).
- ¹⁴E.-J. Kim *et al.*, Phys. Plasmas **11**, 10 (2004).
- ¹⁵A. Ware *et al.*, Plasma Phys. Control Fusion **38**, 1343 (1996).
- ¹⁶W.E. Amatucci *et al.*, Phys. Rev. Lett. **77**, 1978 (1996).
- ¹⁷D. Jassby, Phys. Fluids **15**, 9 (1972).
- ¹⁸W. Gekelman *et al.*, Rev. Sci. Instrum. **62**, 2875 (1991).
- ¹⁹C. Holland *et al.*, Rev. Sci. Inst. **75**, 10 (2004).
- ²⁰S. Zhou *et al.*, Phys. Plasmas **19**, 012116 (2012).
- ²¹E. Powers, Nucl. Fusion **14**, 749 (1974).
- ²²P.W. Terry and D.E. Newman and A.S. Ware, Phys. Rev. Lett. **87**, 185001 (2001).
- ²³M. Umansky *et al.*, Phys. Plasmas **18**, 055709 (2011).
- ²⁴J.M. Beall and Y.C. Kim and E.J. Powers, J. Appl. Phys. **53**, 6, 1982.